Oxygen reduction reaction kinetics of platinum-based catalyst under stress induction

Haibo Jiang,[a] Jiyuan Lu,[a] Liyuan Bi,[a] Lili Zhang,[a] Jiajia Yang,[a] Cui Liu,[a] Shengwei Yu,[*b] Jianhua Shen[*a] and Yihua Zhu[*a]

[a.] Address here. Shanghai Engineering Research Center of Hierarchical Nanomaterials, Key Laboratory for Ultrafine Materials of Ministry of Education, School of Materials Science and Engineering, East China University of Science & Technology, Shanghai 200237, China. E-mail: jianhuashen@ecust.edu.cn; yhzhu@ecust.edu.cn

[b.] School of Chemical Engineering, East China University of Science and Technology, Shanghai 200237, China. E-mail: yushengwei0036@163.com

1. Material and Methods

1.1 Material

Platinum acetylacetonate ($Pt(acac)_2$, 98%), nickel acetylacetonate ($Ni(acac)_2$, 98%), Pb acetylacetonate ($Pb(acac)_2$, 98%), and ethylene glycol ($C_2H_6O_2$, 99%) were purchased from Aladdin Reagent Co., Ltd. Acetone (C_3H_6O, 98%) was purchased from Alfa Aesear. Absolute ethanol and Nifion (ETOH, 95.3%) were from Fisher Scientific. Commercial Pt/C (20 wt% Pt) was purchased from Hesen Electric Co., Ltd. Concentrated perchloric acid ($HClO_4$, 70%) comes from Titan Technology.

1.2 Catalyst preparation process

A 20 mL reaction vial containing 100 mg of Vulcan XC-72 carbon black was placed in an oven and treated at 220 ^{o}C for 24 h. The purpose was to remove the water from the carbon black and ensure its complete drying. 30.8 mg of platinum acetylacetonate ($Pt(acac)_2$) and 6.3 mg of nickel acetylacetonate ($Ni(acac)_2$) were dispersed in 100 μL of a mixture of ethylene glycol and 5 mL of acetone. Then 32 mg of carbon black was dispersed in 8 mL of acetone. Then the mixture containing the metal precursors was slowly added dropwise into the carbon black dispersion using a dropper, and the two distributions were mixed while maintaining sonication conditions. The sonication was performed for 1h to form a uniformly dispersed mixed solution. Then it was transferred to a 25 mL porcelain ark and placed in an oven at 30 ^{o}C for 2 h to dry. Finally, the dried solid was annealed and reduced in a carbon monoxide/hydrogen gas (CO/H_2=24/1) atmosphere. Specifically, PtNi/C was annealed at 300 °C for 2 h and then cooled naturally with a tube furnace heating rate of 5 °C/min and a carbon monoxide flow rate of 120 mL/min. Finally, after the annealing was completed and cooled naturally to room temperature, the samples were removed by purging with argon for 10 min. The PtPb catalyst was synthesized similarly to the PtNi catalyst, except the metal precursors were replaced with acetyl. The PtPb catalyst was synthesized similarly to the PtNi catalyst, except that the metal precursor was replaced with acetylacetonate lead $Pb(acac)_2$, and the other steps remain the same.

1.3 Analysis and Characterization

Transmission electron microscopy (TEM) characterized the surface structure and

morphology of the prepared catalysts. High-resolution electron microscopic images of the samples were collected using a Grand ARM 300F aberration-corrected high Angle ring dark field scanning transmission electron microscope (HAADF). Energy dispersive X-ray spectroscopy (EDX) was used to characterize the elemental distribution. The composition of the nanostructures, as well as the relative fundamental ratios, were determined by inductively coupled plasma atomic emission spectrometry (ICP-AES). A D8 ADVANCE (Bruker, Germany) diffractometer with Cu Kα radiation was used to analyze and determine the crystal structure and phase composition of the prepared catalysts with a scan angle range of 10 – 90^{o}, a scan step of 0.02^{o} and a scan speed of 0.36 s/step.

1.4 Electrochemical testing

Electrochemical experiments were conducted using a CHI760E workstation under a three-electrode system. Preparation of working electrode: 980 μL of isopropanol, 20 μL of Nafion (5 wt%), and 5 mg of catalyst were taken in a small glass vial and ultrasonically dispersed for 1 h to obtain the catalyst ink solution. Then 4 μL ink solution was added dropwise to the working electrode: glassy carbon rotating disc electrode (5 mm diameter) and dried naturally. The graphite electrode was used as the counter electrode, and the saturated glyceryl electrode (SCE) as the reference electrode with the electrode potential conversion relationship: $E_{RHE} = E_{SCE} + 0.242 + 0.0591 \times pH$. The electrochemical test electrolyte under acidic conditions was 0.1 M $HClO_4$ solution.

ORR performance test. Catalyst cyclic voltammetry (CV) curves were tested in

the potential cycling range of 0 - 1.3 V (all potentials in the following are referenced to the reversible hydrogen electrode RHE) at a scan rate of 100 mV s^{-1}, and the electrolyte was a 0.1 M $HClO_4$ solution, into which argon (Ar) was introduced to remove impurity gases before testing. The electrochemical window for the catalyst ORR linear scan curve (LSV) test was 0.1 - 1.23 V. The electrolyte was a 0.1 M $HClO_4$ solution, and the electrolyte solution was fed with O_2 to dissolved saturation before the test at a scan rate of 10 mV s^{-1}. The rotating disk electrode was used to eliminate the effect of mass transfer during the test, and the rotational speed was 1600 rpm. SA was calculated by selecting the current density data at 0.90 V and normalizing the Pt loading and electrochemical activity area (ECSA). The ORR kinetic currents of the catalysts were obtained by the following method. According to the Koutecky-Levich equation:

$$j_k = \frac{j - j_l}{j j_l} \quad (1)$$

Where j_k represents the kinetic current density, j represents the measured current density, and j_l represents the limiting current density, i.e., the diffusion-limited current density (usually the highest current density under relatively negative potentials).[1] The Tafel curve of the reaction was plotted using the logarithm of the kinetic current density as the horizontal coordinate and the electrode potential as the vertical coordinate, where the slope of the fitted straight line is the Tafel slope.

Apparent activation energy. First, the electrolyte was poured into the inner layer of the four-port jacketed electrolytic cell. Then circulating water was fed into the outer layer of the jacketed electrolytic cell using a thermostatic water bath and maintained at

a specific temperature. A calibrated alcohol thermometer measured the electrolyte temperature. The catalyst ORR polarization curves were obtained at 278.15, 288.15, 298.15, 308.15, and 318.15 K, respectively. According to the Arrhenius and Bulter-Volmer equations, the oxygen reduction reaction kinetic currents were calculated with test voltages of 0.05 ~1.23 V, a scan rate of 0.1 V s^{-1}, and a rotating disc speed of 1600 rpm.

$$k = A\exp\left(-\frac{E_a}{RT}\right) \tag{2}$$

$$j_k = nFkc \tag{3}$$

Where k represents the reaction rate constant, A represents the prefactor, Ea represents the apparent activation energy of the reaction, R represents the gas constant, T represents the reaction temperature, j_k represents the kinetic current density, n represents the number of electrons transferred by the reaction, F represents the Faraday constant, and c represents the concentration of the reactants.

$$\ln j_k = -\frac{E_a}{RT} + \ln(cnFA) \tag{4}$$

The graph is drawn with 1/T as the horizontal coordinate and ln jk as the vertical coordinate. The slope of the fitted line is $-E_a/R$, from which the apparent activation energy Ea of the reaction can be obtained.

Reaction order of H^+. The pH of the electrolyte is adjusted by changing the $HClO_4$ concentration in the pH range of 1-3, and the ClO_4^- concentration is kept

constant by using $KClO_4$. LSV tests obtain polarization curves and kinetic current densities. The logarithm of the kinetic current density was used as the vertical coordinate, and the logarithm of the H^+ concentration was used as the horizontal coordinate for the graph. The slope of the straight line fitted at different potentials is H^+ reaction order.

1.5 Electrochemical *in-situ* infrared testing

In-situ IR spectra were obtained by the following method. The prepared catalyst ink was added dropwise to a silicon column coated with a gold film, and the IR spectra were collected in oxygen-saturated 0.1 M $HClO_4$ solution and argon saturated 0.1 M $HClO_4$ solution using a constant potential measurement mode with a potential interval of 0.05 V from open circuit potential (OCP) to 0.05 V. The test time was 80 s. The oxygen or argon gas was maintained during the test pass-through.

2. DFT calculation

This chapter's theoretical calculations are based on the first-principle measures of density generalized function theory. They are simulated using the Materials Studio software configured with the $DMOL_3$ module and the CASTEP package. The calculations of electronic structure and exchange-related effects are based on the generalized gradient approximation and the Perdew-Burke-Ernzerhof (GGA-PBE) function. The DNP function expands the valence electrons. The inner electrons are held in place by the semi-nuclear pseudopotential. The model is built based on structural features and simulated using four-layer periodic cells, where the two atomic layers at

the bottom of the model are fixed, the other atoms are entirely relaxed, and the vacuum layer is set to 10 Å. In the ice-like adsorption model, the structural model of the pure Pt catalyst is modeled using a 4 × 4 (111) four-layer slab model with cells repeated in 2 × 2 × 2 cells. To calculate the results more accurately, zero-point potential energy (ZPE) correction was applied to all the calculated results, and the model structure was optimized. The flat plate models of PtNi alloy and PtPb alloy were made by randomly replacing the Pt atoms in the Pt flat plate model with Ni and Pb atoms. A 3 × 4 (111) four-layer plate model was used without changing other setup options, ensuring that the Pt/Ni, Pt/Pb Pt/Pb atomic ratios are the same as those of the prepared catalyst.

The $4e^-$ reaction process of ORR consists of four basic reaction steps.

$$O_2 \rightarrow *O_2 \quad (5)$$

$$*O_2 + H^+ + e^- \rightarrow *OOH \quad (6)$$

$$*OOH + H^+ + e^- \rightarrow *O + H_2O \quad (7)$$

$$*O + H^+ + e^- \rightarrow *OH \quad (8)$$

$$*OH + H^+ + e^- \rightarrow H_2O \quad (9)$$

Three intermediate products, *OOH, *O, and *OH, are produced during the reaction.

The free energy change in the ORR process was calculated according to the following equation:

$$\Delta G_1 = \Delta G(*OOH) - (4.92\ \text{eV} - 4\ \text{eU}) \quad (10)$$

$$\Delta G_2 = \Delta G(*O) - \Delta G(*OOH)$$

(11)

$$\Delta G_3 = \Delta G(*OH) - \Delta G(*O)$$

(12)

$$\Delta G_4 = - \Delta G(*OH)$$

(13)

The free energy of each of the adsorbed substances is given by:

$$\Delta G(ad) = \Delta E(ad) + \Delta ZPE(ad) - T\Delta S(ad) + (x - 4)\,eU$$

(14)

Where ΔG (ad) is the change in free energy before and after adsorption, ΔE (ad) is the adsorption energy, ΔZPE (ad) is the zero-point energy, TΔS (ad) is the effect of the entropic change. X is the total number of electron transfers. Since the adsorption of a monolayer of water is considered in the model, the dissolution energy is not considered separately.

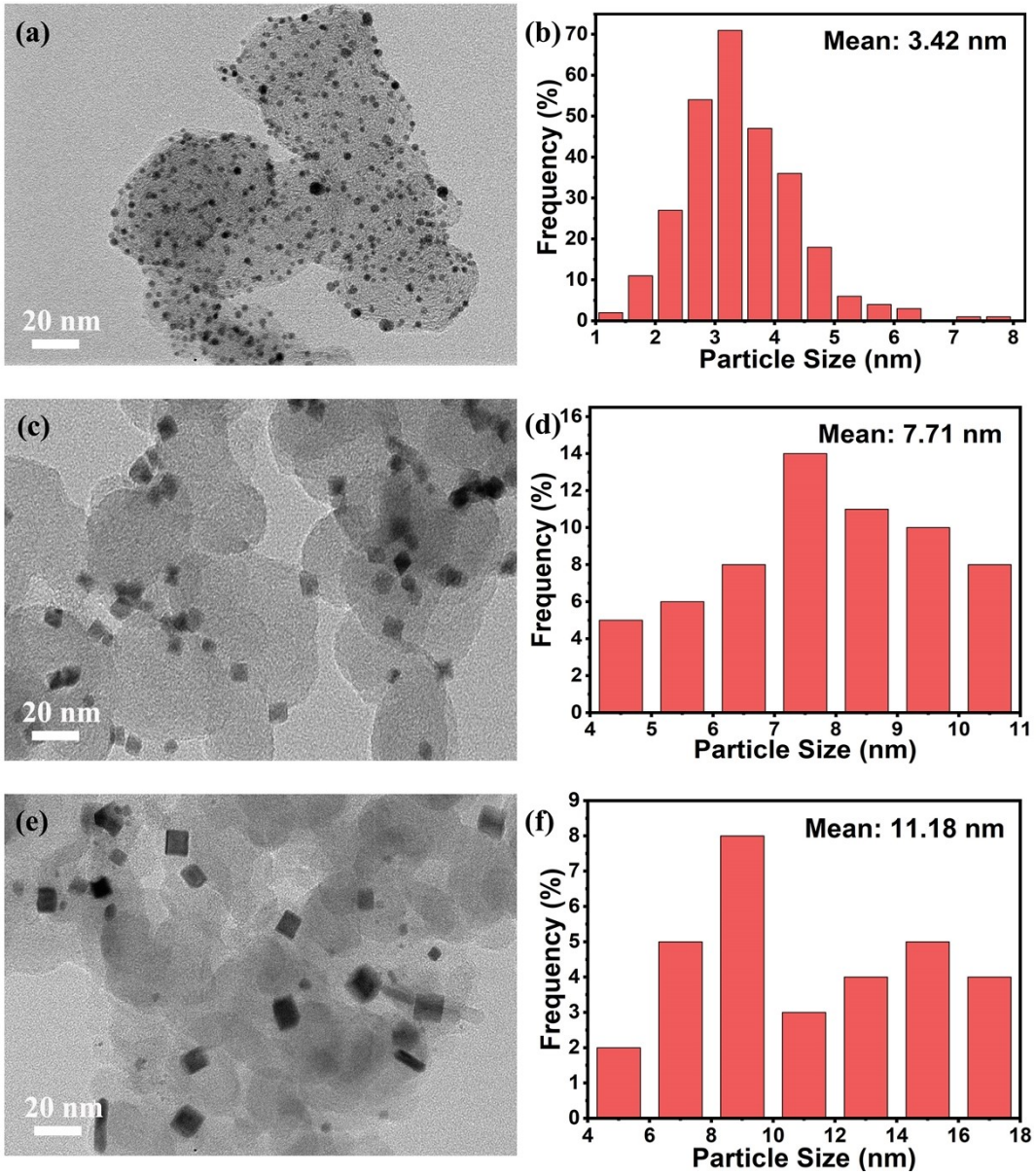

Fig. S1. TEM characterization: (a) commercial Pt/C, (c) PtNi and (e) PtPb. Histogram of particle size distribution: (b) commercial Pt/C, (d) PtNi and (f) PtPb.

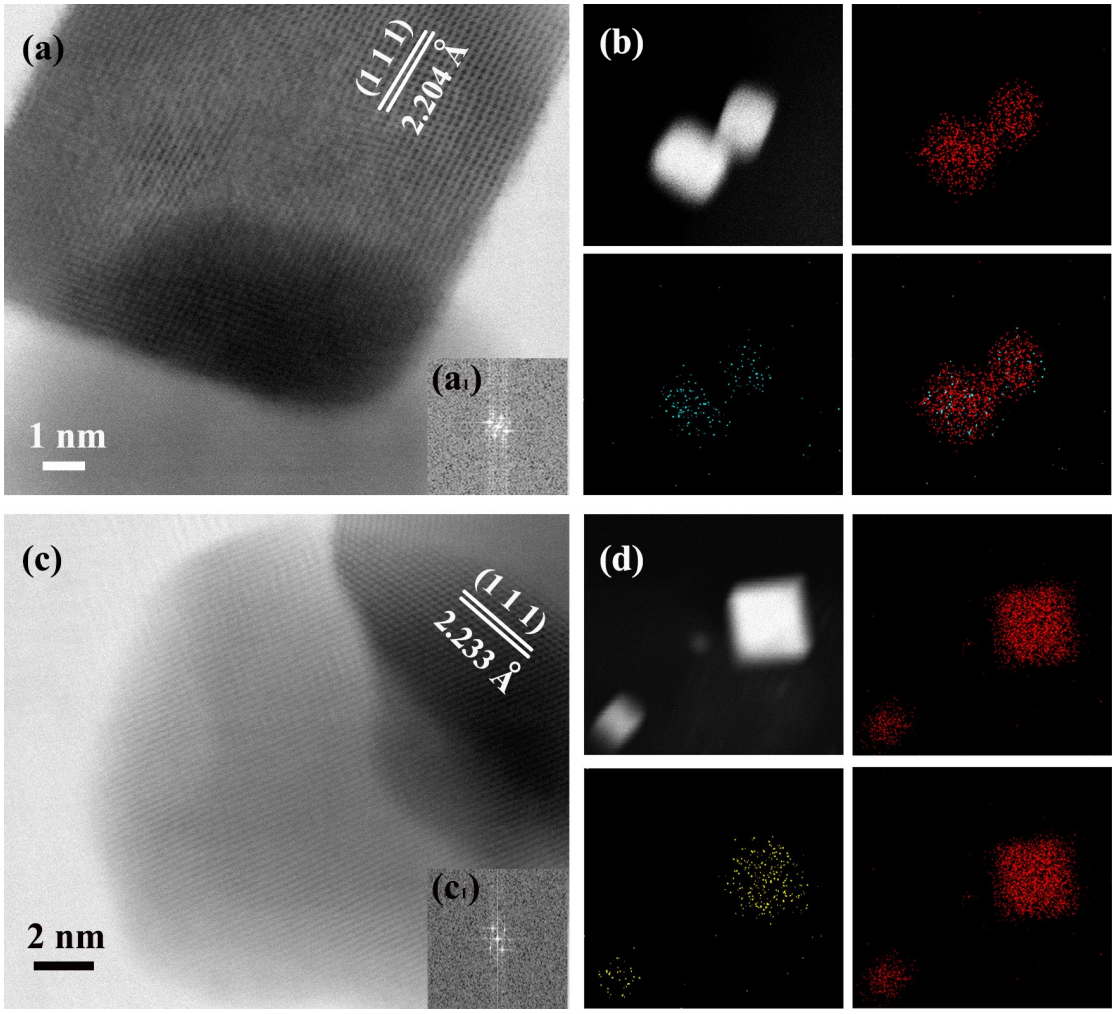

Fig. S2. HAADF STEM image of (a) PtNi and (c) PtPb. STEM-EDS mapping of (b) PtNi and (d) PtPb.

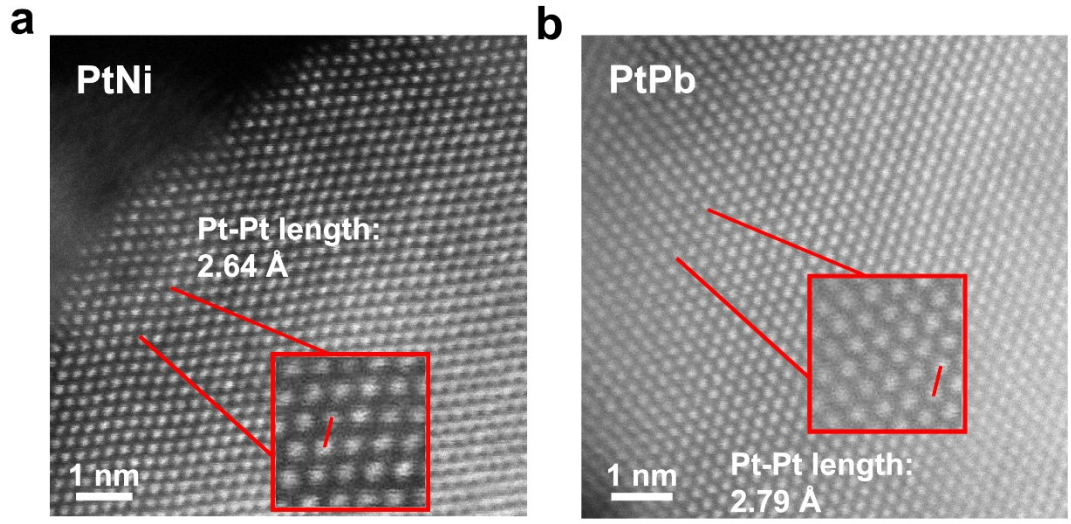

Fig. S3. The high-angle annular dark-field scanning transmission microscopy (HAADF-STEM) of **(a)** PtNi and **(b)** PtPb catalysts, respectively.

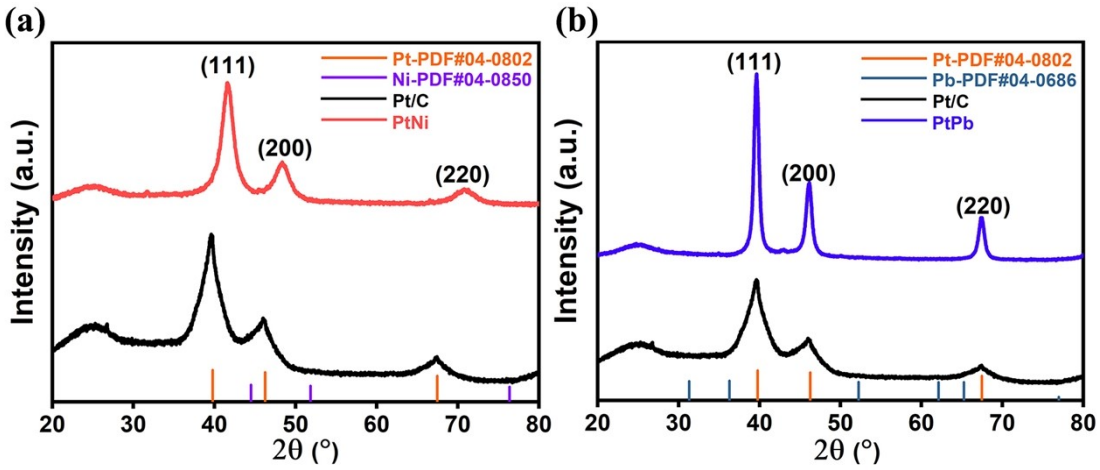

Fig. S4. XRD comparison of PtNi (a) and PtPb (b).

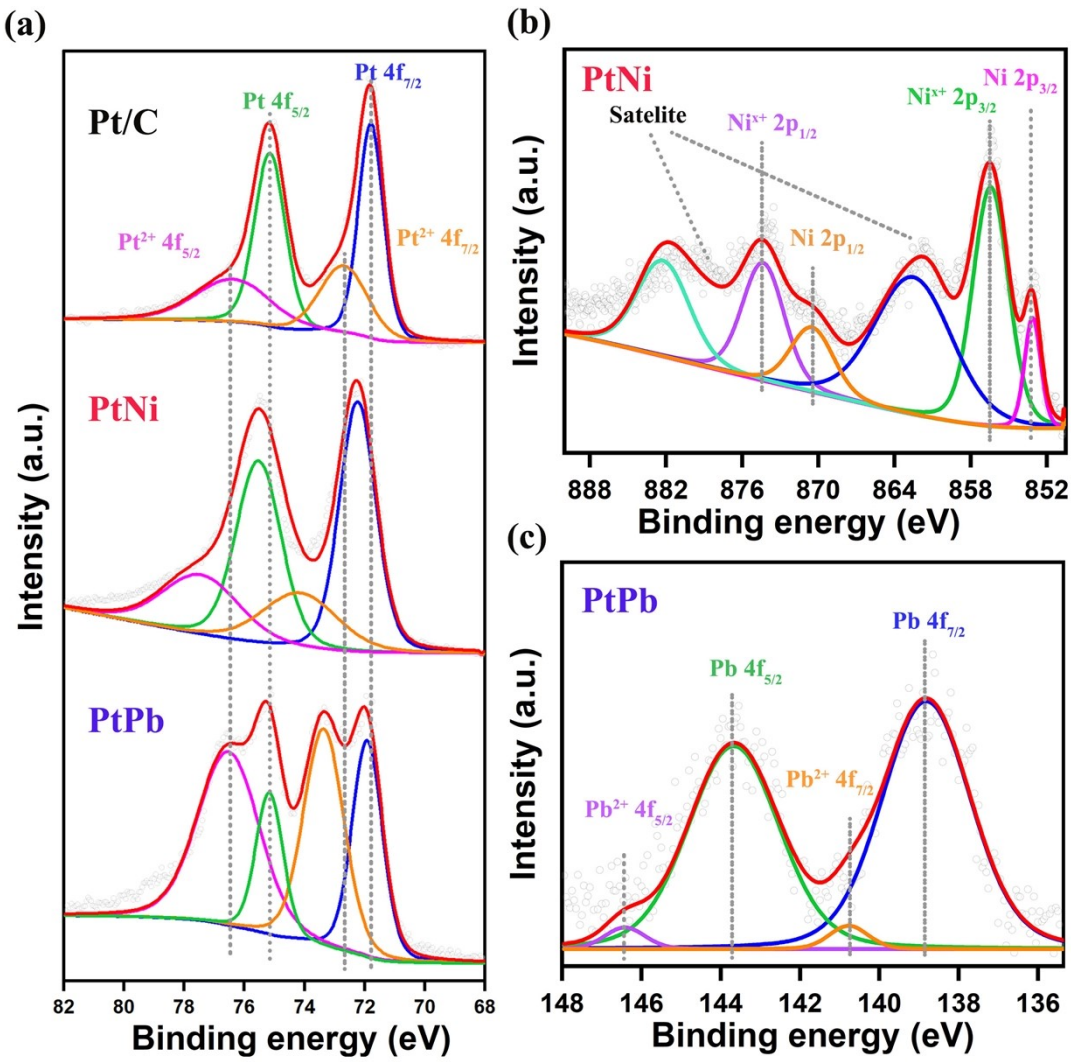

Fig. S5. (a) Comparative Pt *4f* XPS patterns of commercial Pt/C, PtNi, and PtPb; (b) Ni *2p* XPS patterns of PtNi; (c) Pb *4f* XPS patterns of PtPb.

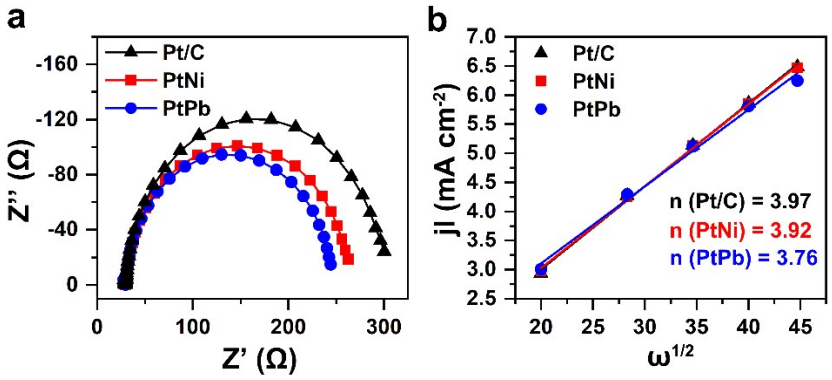

Fig. S6 (a) The EIS plots for commercial Pt/C, PtNi and PtPb, respectively. (b) The relationship between the limiting current density (jl) and the 1/2 power of the rotation speed (ω) according to the KL equation, the number of electrons transferred for commercial Pt/C, PtNi and PtPb -catalyzed ORR, based on the slope of the fit, is 3.97, 3.92 and 3.76, respectively.

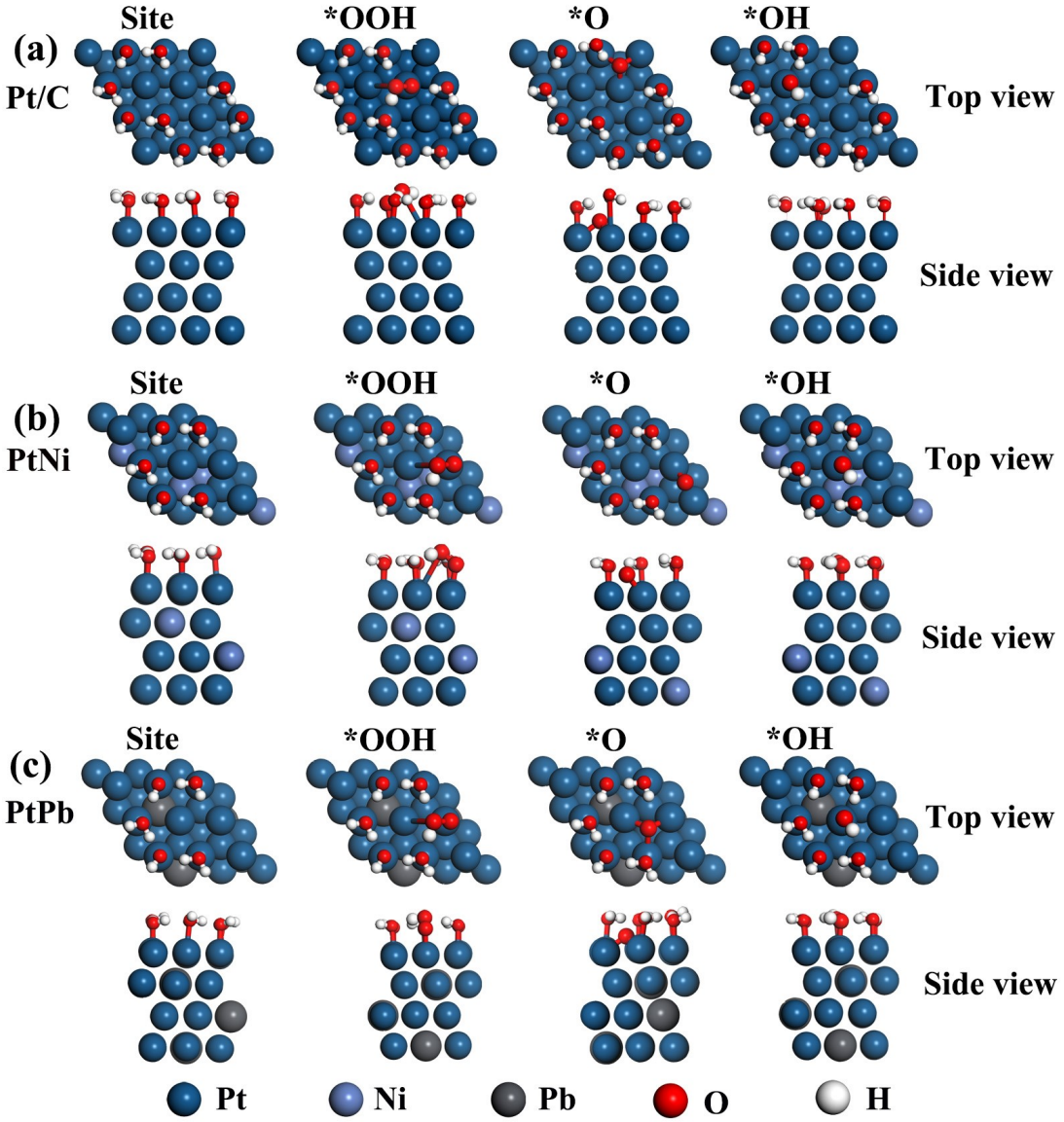

Fig. S7. Top and side views of the calculated model of the oxygen-containing products involved in the free energy theory calculation of the ORR. (a) pure Pt(111); (b) PtNi(111); (c) PtPb(111). The blue, purple, gray, red and white spheres represent Pt, Ni, Pb, O, and H atoms, respectively.

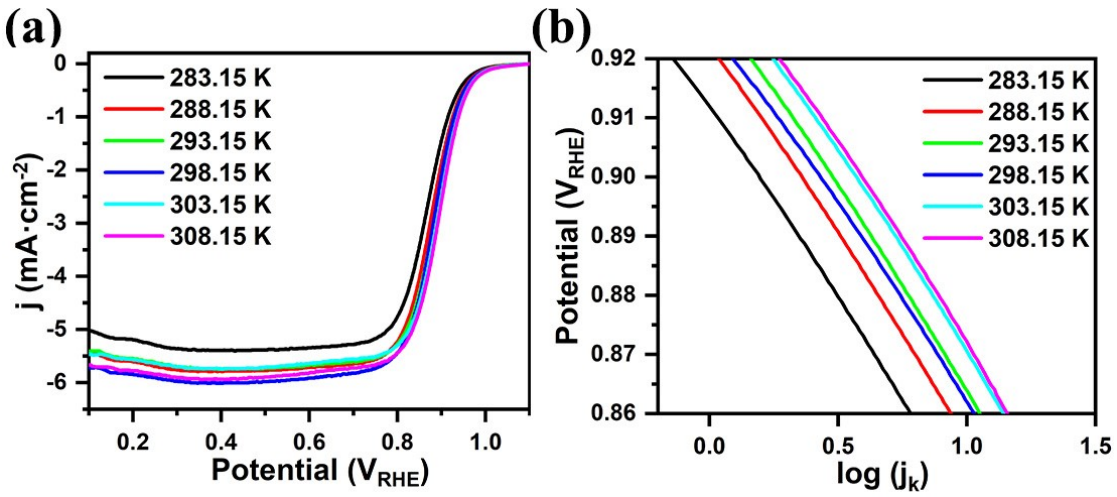

Fig. S8. Commercial Pt/C at different reaction temperatures (a) ORR polarization curves; (b) Tafel curves.

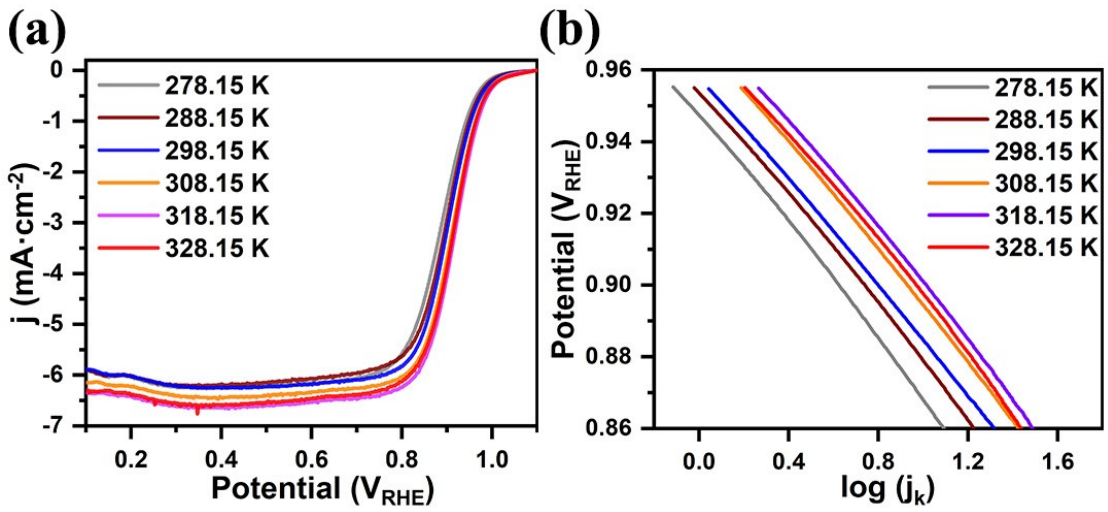

Fig. S9. PtNi at different reaction temperatures (a) ORR polarization curves; (b) Tafel curves.

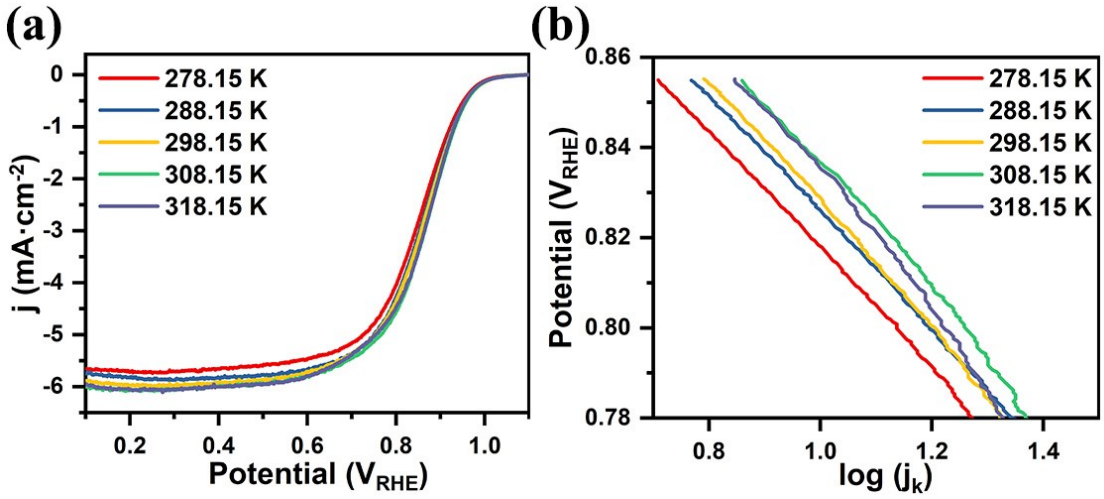

Fig. S10. PtPb at different reaction temperatures (a) ORR polarization curves; (b) Tafel curves.

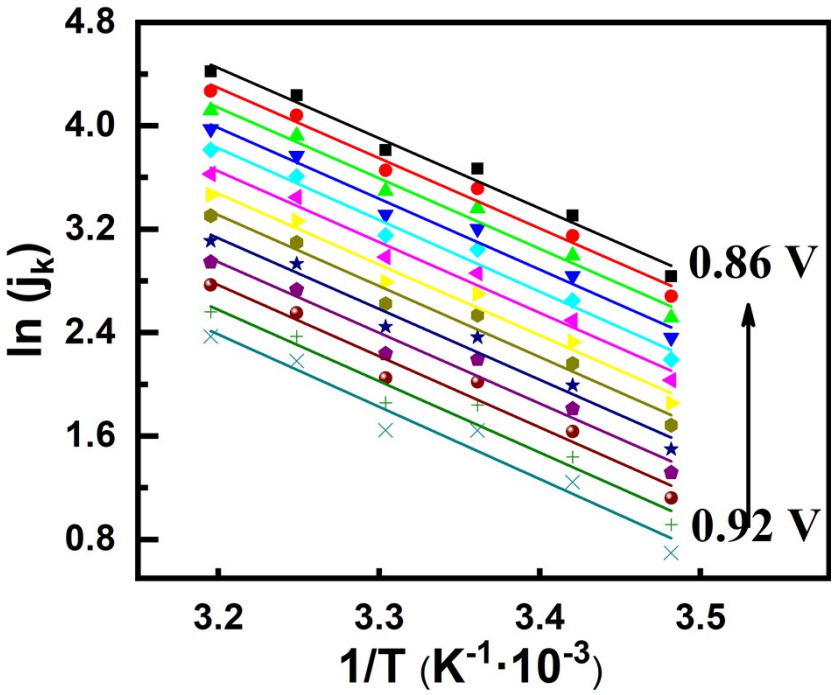

Fig. S11. Raw data of Commercial Pt/C for calculating the apparent activation energy of a reaction. Relationship between the logarithm of the kinetic current density and the inverse of the temperature. PtNi ;(c) PtPb.

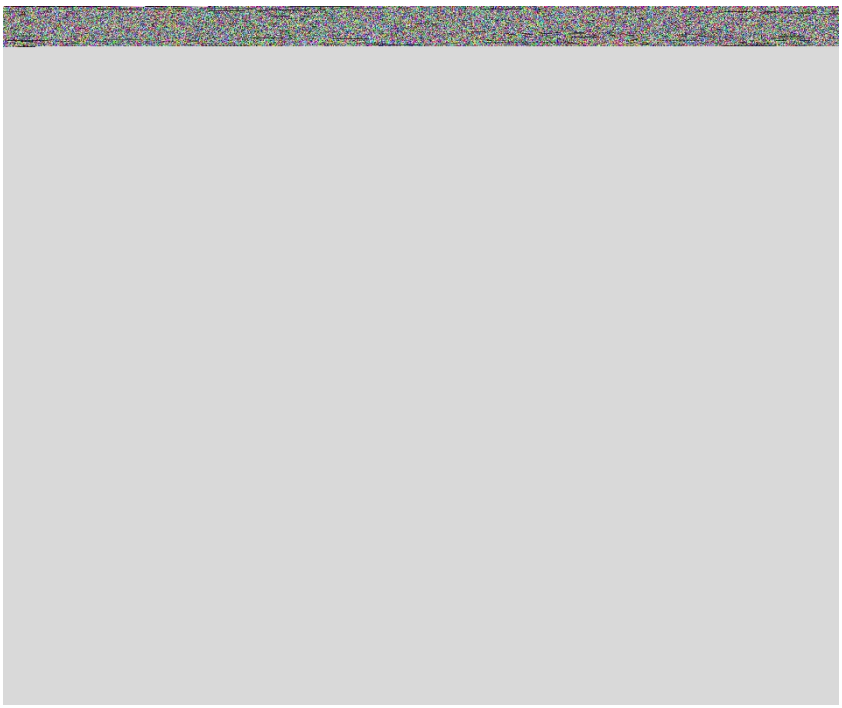

Fig. S12. Raw data of PtNi for calculating the apparent activation energy of a reaction. Relationship between the logarithm of the kinetic current density and the inverse of the temperature.

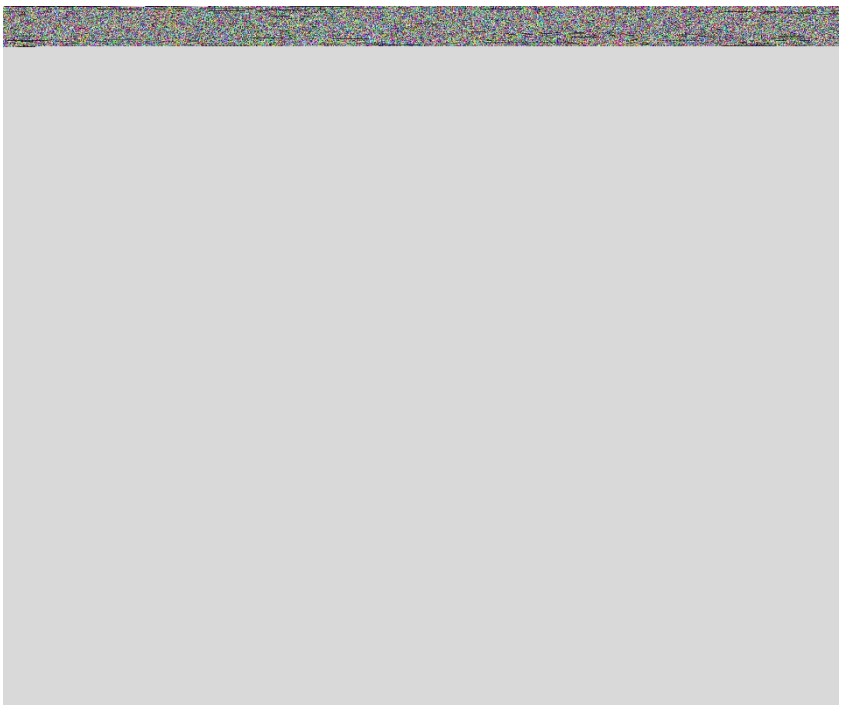

Fig. S13. Raw data of PtPb for calculating the apparent activation energy of a reaction. Relationship between the logarithm of the kinetic current density and the inverse of the temperature.

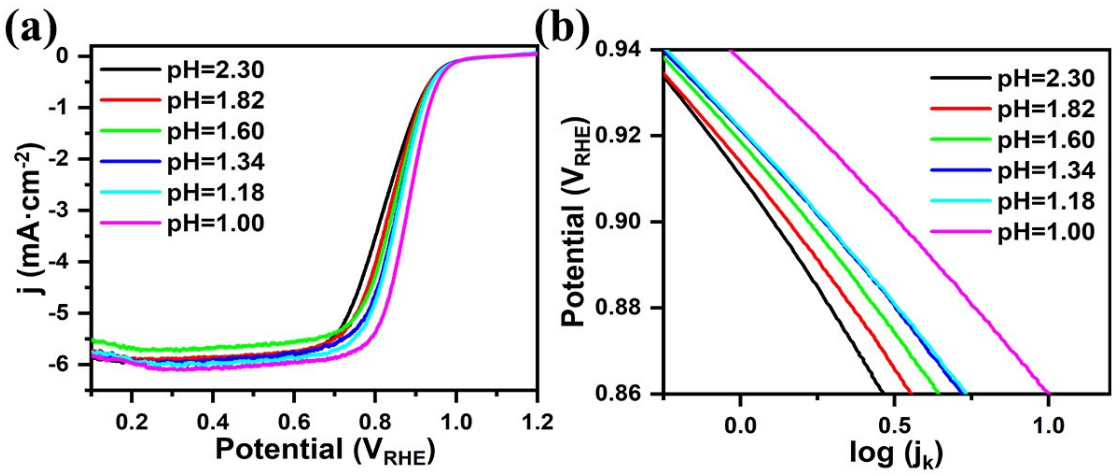

Fig. S14. Commercial Pt/C at different reaction pHs (a) ORR polarization curves; (b) Tafel curves.

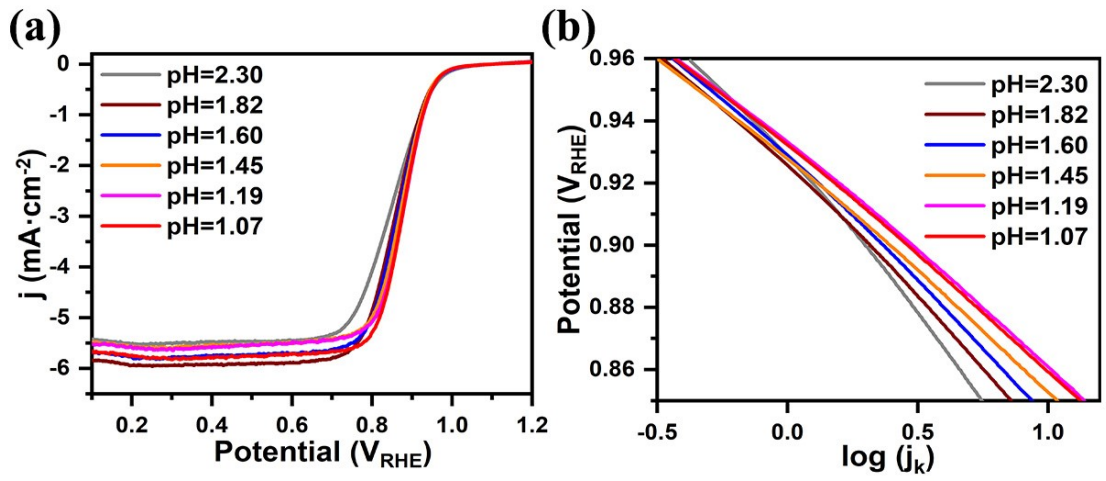

Fig. S15. PtNi at different reaction pHs (a) ORR polarization curves; (b) Tafel curves.

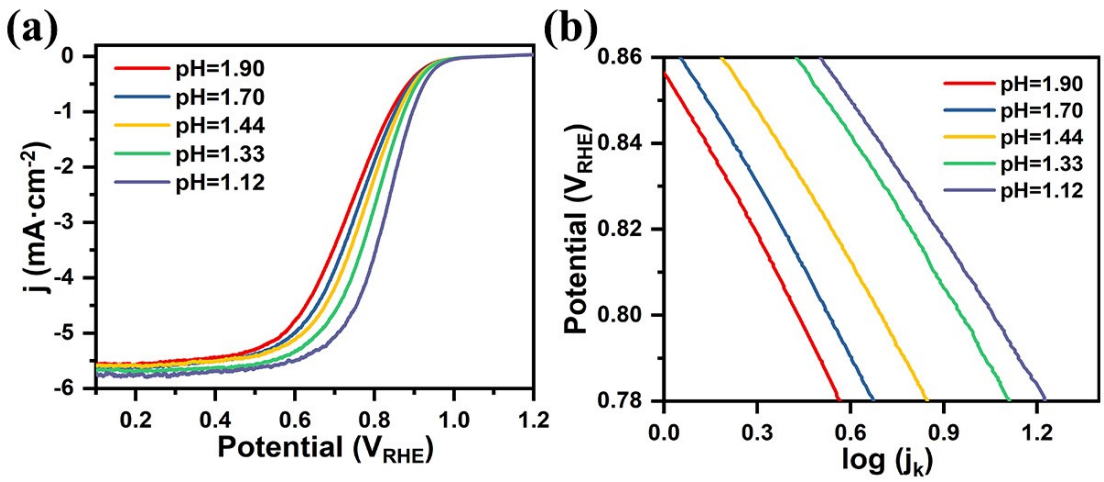

Fig. S16. PtPb at different reaction pHs (a) ORR polarization curves; (b) Tafel curves.

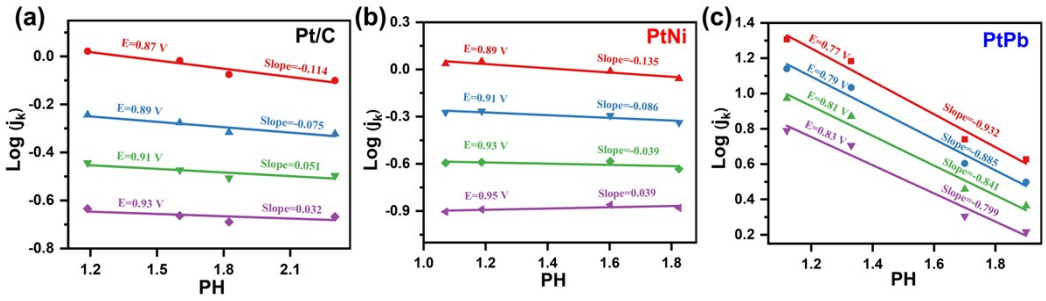

Fig. S17. ORR reaction order test results. (a), (b) and (c) are the H^+ reaction orders of commercial Pt/C, PtNi, and PtPb at different potentials.

Table S1 Comparison of catalyst performance and the ORR kinetic properties among this work and recent reports on ORR catalysts

Catalysts	E_{onset} (V vs. RHE)	$E_{1/2}$ (V vs. RHE)	Tafel slope (mV dec^{-1})	RDS	Reference
PtNi	0.97	0.90	69	*OOH→*O+*OH	This work
PtPb	0.88	0.81	124	$O_2+H^++e^-$→*OOH	This work
Pt/C	0.93	0.86	68	*OOH→*O+*OH	This work
O-$PtCo_3$@HNCS	0.92	0.84	~ 60	*OOH→*O+*OH	[2]
O-$PtCo_3$/HNCS	0.90	0.82	~ 62	*OOH→*O+*OH	[2]
Pt (111)	0.90	0.85	60	*OOH→*O+*OH	[3]
meso-i-Ga_3Pt_5	0.86	0.80	65.3	*OOH→*O+*OH	[4]
Pt_{NP}−Mn_{SA}/C	0.94	0.90	40.1	*O+H^++e^-→*OH	[5]
Fe–N–C/Pd	0.97	0.87	51.1	*OOH→*O+*OH	[6]
Fe–N–C	0.91	0.81	57.1	*OOH→*O+*OH	[6]

Table S2. Reaction-free energy changes of oxygen reduction radicals on the surfaces of Pt(111), PtNi(111), and PtPb(111)

Model	U	O_2→*OOH	*OOH→*O	*O→*OH	*OH→H_2O
Pt(111)	0 V	−1.34	−1.81	−0.88	−0.89
	1.23 V	0.11	0.58	0.36	0.34
PtNi(111)	0 V	−1.29	−1.49	−1.12	−1.02
	1.23 V	0.66	0.26	0.11	0.21
PtPb(111)	0 V	−1.38	−1.86	−0.82	−0.86
	1.23 V	0.15	0.21	0.01	−0.37

Table S3. DFT-calculated ΔE (ad) values of Pt(111), PtNi(111), and PtPb(111) under an acidic environment, ZPE, and TS for adsorbates.

Model	Species	ΔE (eV)	ZPE (eV)	TS (eV)
Pt(111)	*OOH	3.08	0.24	0
	*O	1.72	0.23	0
	*OH	0.44	0.02	0
	*	0	0	0
PtNi(111)	*OOH	3.13	0.25	0
	*O	2.07	0.22	0
	*OH	0.56	0.02	0
	*	0	0	0
PtPb(111)	*OOH	3.06	0.26	0
	*O	1.53	0.13	0
	*OH	0.41	0.03	0
	*	0	0	0

Reference

1. Wang, X.; Li, Z.; Qu, Y.; Yuan, T.; Wang, W.; Wu, Y.; Li, Y., Review of Metal Catalysts for Oxygen Reduction Reaction: From Nanoscale Engineering to Atomic Design. *Chem* **2019,** *5* (6), 1486-1511.

2. Hu, Y.; Guo, X.; Shen, T.; Zhu, Y.; Wang, D., Hollow Porous Carbon-Confined Atomically Ordered PtCo3 Intermetallics for an Efficient Oxygen Reduction Reaction. *ACS Catalysis* **2022,** *12* (9), 5380-5387.

3. Luo, M.; Koper, M. T. M., A kinetic descriptor for the electrolyte effect on the oxygen reduction kinetics on Pt(111). *Nature Catalysis* **2022,** *5* (7), 615-623.

4. Lv, H.; Zheng, Y.; Wang, Y.; Wang, J.; Liu, B.; Qiao, Z. A., Ordered Mesoporous Intermetallic Ga-Pt Nanoparticles: Phase-Controlled Synthesis and Performance in Oxygen Reduction Electrocatalysis. *Angewandte Chemie International Edition* **2023,** *62* (24), e202304420.

5. Wei, X.; Song, S.; Cai, W.; Kang, Y.; Fang, Q.; Ling, L.; Zhao, Y.; Wu, Z.; Song, X.; Xu, X.; Osman, S. M.; Song, W.; Asahi, T.; Yamauchi, Y.; Zhu, C., Pt Nanoparticle–Mn Single-Atom Pairs for Enhanced Oxygen Reduction. *ACS Nano* **2024,** *18* (5), 4308-4319.

6. Wei, X.; Song, S.; Cai, W.; Luo, X.; Jiao, L.; Fang, Q.; Wang, X.; Wu, N.; Luo, Z.; Wang, H.; Zhu, Z.; Li, J.; Zheng, L.; Gu, W.; Song, W.; Guo, S.; Zhu, C., Tuning the spin state of Fe single atoms by Pd nanoclusters enables robust oxygen reduction with dissociative pathway. *Chem* **2023,** *9* (1), 181-197.